Steel and Composite Structures, *Vol. 26, No. 1 (2018) 55-66*
DOI: https://doi.org/10.12989/scs.2018.26.1.055

Numerical evaluation of buried composite and steel pipe structures under the effects of gravity

William Toh, Long Bin Tan, Kwong Ming Tse, Karthikayen Raju,
Heow Pueh Lee and Vincent Beng Chye Tan*

Department of Mechanical Engineering, National University of Singapore, 117578, Singapore

(*Received June 30, 2017, Revised September 12, 2017, Accepted September 25, 2017*)

Abstract. In this paper, the response of an underground fibreglass reinforced plastic (FRP) composite pipe system subjected to realistic loading scenarios that may be experienced by an actual buried pipeline is investigated. The model replicates an arbitrary site with a length of buried pipeline, passing through a 90° bend and into a valve pit. Various loading conditions, which include effects of pipe pressurization, differences in response between stainless steel and fibreglass composite pipes and severe loss of bed-soil support are studied. In addition to pipe response, the resulting soil stresses and ground settlement are also analysed. Furthermore, the locations of potential leakage and burst have also been identified by evaluating the contact pressures at the joints and by comparing stresses to the pipe hoop and axial failure strengths.

Keywords: fibreglass reinforced plastic (FRP); composite pipe; FE modeling; geostatic loading

1. Introduction

In recent years, due to rapid urbanization, there has been a steady increase in the utilization of fluid transportation systems. Fluid transportation systems, according to hydraulic theories, may be classified as either open channel flow or pipe flow. Although open channel flows are less costly and easier to implement, buried pipelines remain a popular option as pipe flow is more controllable and less reliant on environmental factors, such as the need for gravity assist.

Buried pipelines can generally be classified into rigid and flexible pipes (Watkins and Anderson 1999). Both fibreglass reinforced plastic (FRP) and steel pipes fall into the category of flexible pipes. While steel has been a conventional material of choice for buried pipelines, there has been increasing utilization of FRP in replacing steel as the choice material for buried pipelines. This is due to the reduction in costs of composite materials, which was once an inertia in large scale usage of this material, despite excellent properties such as high strength-to-weight ratio, corrosion resistance and low coefficient of thermal expansion, to name a few (Jones 1998, Armstrong *et al*. 2005, Beckwith and Greenwood 2006, Taheri 2013). With a growing number of energy pipeline constructions globally, there is a need to have a better understanding of the 3D effects of environmental loading conditions on these piping systems. One common 3D environmental effect is the effect of topsoil overburden, which is the downward pressure caused by the weight of soil above a particular depth. This deeper understanding will allow for better design aspects of future pipelines, which will reduce maintenance costs.

With the increasing construction of energy pipeline projects around the world, where some pipeline routes may need to cross environmentally sensitive areas, there is a growing need to improve the understanding of 3D effects in deformable pipes composed of steel or composite materials, for example due to seismic activities (Gantes and Melissianos 2016), live traffic loads (Chapman *et al*. 2016), blast loads (Soheyli *et al*. 2016) and buckling due to uncertainty effects in soil (Khemis *et al*. 2016).

Unlike most metallic systems, it is necessary to calculate the potential pressure expansion in fibreglass reinforced plastic (FRP) piping systems due to their low moduli, especially those manufactured with E-glass fibres, which may be over 10 times less than their traditional metallic counterparts. FRP products can have a pressure expansion that is 25 times greater than carbon and stainless steels (Schmmit 1998) and can potentially affect many design properties as well as on adjacent soil disturbance due to cyclic pressurization. In addition to mechanical properties, FRP pipes offer better thermal insulation as compared to their metallic counterparts (Chen *et al*. 2014).

Numerous literature has been focusing on the response of pipelines or pressure vessels, most of which were focused on hydrostatic loads (Gong and Hu 2014, Bai *et al*. 2016, Rafiee and Mazhari 2016), which is skewed towards deep-water applications rather than buried pipelines.

Parametric studies on buried composite pipelines under various loading scenarios have been presented in recent years (Olarewaju *et al*. 2010, Olarewaju *et al*. 2010, Olarewaju *et al*. 2010, Olarewaju *et al*. 2010, Almahakeri *et al*. 2012), but they were simplistic models that were either mostly with limited pipe lengths (Lee *et al*. 2015), or were "smooth" pipes that did not incorporate joint connections or pipe bends (Vazouras *et al*. 2010, Trifonov and Cherniy

*Corresponding author, Associate Professor
E-mail: mpetanbc@nus.edu.sg

http://www.techno-press.org/?journal=scs&subpage=6
ISSN: 1229-9367 (Print), 1598-6233 (Online)

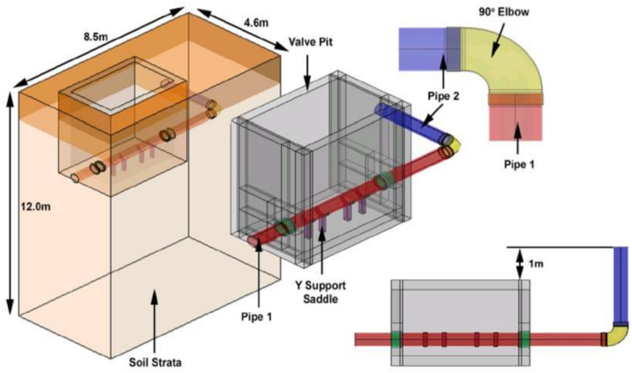

Fig. 1 Geometrical details of the model

2012, Vazouras *et al*. 2012). Although some literature investigated environmental factors affecting pipelines, such as the spatial variability of buried pipes (Elachachi *et al*. 2012), soil expansion (Rajeev and Kodikara 2011), poor haunch support on rigid pipes (Alzabeebee 2016), seismic faults (Gantes and Melissianos 2016) and uplift resistance (Mahdi and Katebi 2015), the authors were unaware of any works on the practical consideration of loss of bed-soil support.

Olarewaju *et al*. (2010) found that for both surface and underground loads, the pipe displacements may change when the Young modulus of soil is varied. For soil modulus from 10 kPa to 1000 kPa, his simulation results predicted increasing pipe pressure, stress and strain. The crown has the highest absolute stress and strain while the invert has the maximum pressure. This is in agreement with Liu (2009) who showed that as the modulus of soil increases, greater stresses are transmitted more efficiently over a further distance to reach the buried pipe.

For varying pipe stiffness, Olarewaju *et al*. (2010) showed that low stiffness PVC or clay pipes yielded higher pipe displacement at the crown but lower values at the invert and spring-lines during ground surface loading. However, for stiffer steel or reinforced concrete pipes, the resulting pipe wall displacements were more equal. Pipe pressures and stresses were also found to increase with higher pipe stiffness, while the resulting strains are reduced. For low stiffness pipes, high localised deformations at the joints may also cause leakage. When the bed soil is firm, hardly any subsidence takes place hence the pipe stiffness may not be crucial. However, when the bed is loose or soft, subsidence becomes a real issue and can affect the integrity of softer underground pipelines if they are not suitably reinforced. It was also reported that increasing the burial depth enhances the confinement on the pipe which reduces the maximum displacement, stress and strain under many loading scenarios (Liu 2009, Olarewaju *et al*. 2010).

In this paper, the effects of topsoil overburden on both stainless steel and composite pipes under operating (pressurized) and non-operating (unpressurized) conditions are studied. This analysis allows for a deeper understanding of the difference in response of pipelines of the two materials, as well as identifies possible locations of leakage and burst. In addition, the effects of loss of bed soil support will also be investigated. This scenario forms a simplified analysis of the effects of severe geotechnical catastrophes, such as earthquakes and landslides, which are likely to cause the pipe network to lose support.

Table 1 Number of elements and materials for each component

Components	No. of elements	Material
90° elbow	5520	FRP
MCT module	84968	EPDM rubber
Pipe	18360	FRP
Soil	359718	5 strata of soil
Valve pit	40880	Concrete
Y support saddle	1796	Steel
Total	511242	-

2. Materials and method

2.1 FE Modelling

The model comprises a cuboid valve pit of dimensions 3.8 m×2.6 m×4.3 m ($L\times W\times D$), with five sides having thick concrete walls and its top side being open. The distance between the pipe's top surface and the pit floor is approximately 1 m. During operation, the pipe, of nominal diameter of d_0, is pressurized with an internal pressure of P_0, simulated by a pressure load on the internal surfaces of the pipe. At the pipe-pit penetration, there is a mass-cable transit (MCT) module, which consists of thick rubber seals tightened by steel frames. This allows the pipes to be clamped and secured. To accommodate properties of different soil layers depth-wise, the soil is divided into five strata with different assigned soil parameters. The three-dimensional (3D) finite element models are shown in Fig. 1. In the current model, the burial depth and operating pressure modelled are representative of typical pipeline systems and thus parametric studies for varying burial depths and operating pressures are not conducted.

2.2 Material properties

Except for the FRP pipes and MCT rubber seals, all other components adopt linear elastic, isotropic material properties. The Mohr-Coulomb plasticity soil model is used where the required parameters are estimated from information given by actual soil investigation reports

The number of solid elements and material properties for each component in the models are shown in Table 1 and Table 2 respectively.

2.3 Interaction, boundary conditions and soil loading

Contact interactions between the various components are modelled with a tangential sliding behaviour and normal hard contact. The coefficient of friction between these surfaces is assumed to be 0.2. Although a uniform friction coefficient value is used throughout the entire model, there is little effect on calculation effects when these values are changed to suit each and every interaction surface pair as

Table 2 Material properties used in simulation

Material	Young's modulus, (MPa)	Poisson's ratio	Friction angle	Density, (ton/mm^3)
Concrete	27535	0.17		2.40×10^{-9}
Steel	210000	0.3		7.85×10^{-9}
1st soil stratum	6.56	0.15	28	1.60×10^{-9}
2nd soil stratum	9.38	0.1875	28.4	1.68×10^{-9}
3rd soil stratum	49.58	0.225	34	1.75×10^{-9}
4th soil stratum	66.25	0.2625	37.9	1.83×10^{-9}
5th soil stratum	75.21	0.3	40	1.90×10^{-9}

	E_1	E_2	E_3	v_{12}	v_{13}	v_{23}	G_{12}	G_{13}	G_{23}	
							Shear modulus (MPa)			
FRP (Tan *et al.* 2015)	4430	25200	11400	0.04	0.12	0.56	2960	1910	12800	1.90×10^{-9}

Mooney-Rivlin hyperelastic model							
	C10 (MPa)	C01 (MPa)	C20 (MPa)	C02 (MPa)	D1 (MPa^{-1})	D2 (MPa^{-1})	
EPDM (Song and Chen 2003)	20.7107	4.4321	0	0.0771	1.96133×10^{10}	1.96133×10^{10}	1.46×10^{-9}

Table 3 Scenarios investigated using finite element model developed

	Pipe material	Soil condition below pipe
Scenario 1	Stainless steel	Fully supported
Scenario 2	FRP	Fully supported
Scenario 3	FRP	Partially supported due to loose bed-soil

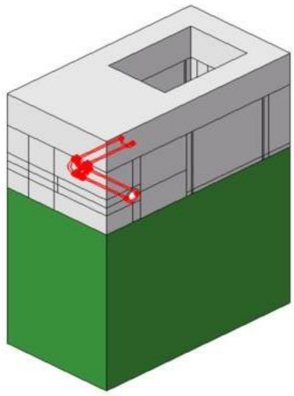

Fig. 2 A schematic of the affected pipe segment which has weaker underlying soil properties to study the effect of loss in bed-soil support

there is limited relative motion between these surfaces. In a separate simulation repeated using higher friction coefficients, in the range of 0.5-0.6, the results differ by less than 1% from the current set of simulation results. In addition, due to the relatively small displacement of soils at the soil-pipe interface, these surfaces are assumed to be always in contact with each other, and are hence assigned tie constraints.

The four vertical faces of the soil model are assigned zero normal displacement to assimilate lateral constrain of the soil, whereas the bottom surface is rigidly fixed to simulate the hard stratum beneath the depth of 16 m. The depth of 16 m is obtained through Standard Penetration Tests from soil investigation reports (BRYAN 1956, V-PILE 2011) from actual sites.

Joints between the composite pipes and the elbow are modeled using a bell-spigot connection (Ameron 2008) whereas joints between the stainless steel pipe components are modeled using tie interactions. To hold the pipe in place within the pipe-pit penetration, a rubber seal is tightened between two steel frames. The steel frames are compressed with a pressure of 1.49 MPa pressure to create sealing pressure of about 500 kPa between the pipe and the pit. The stresses induced through the interference fit have been investigated in an earlier work (Tan *et al*. 2015) and will not be elaborated in this paper.

2.4 Scenarios studied

Using the finite element model described, three possible scenarios are investigated. Scenarios 1 and 2 allow for a direct comparison of the responses of pipes made of stainless steel and FRP. Scenario 3 studies the effects of having loose bed-soil support beneath the pipe. Table 3 summarizes the differences between the three scenarios modelled.

For simulation of loose bed-soil support, the soil directly below the buried pipeline that is outside of the pit are prescribed with one-tenth of its original soil elasticity and density to simulate the critical case of severe loss of bed-soil support. This affected segment of the pipeline is about 6.0 m long and spans from the pit-pipe penetration to the end edge of the model, inclusive of the 90 degree elbow (see Fig. 2).

3. Results and discussion

3.1 Differences with stainless steel pipe

The differences in soil response under the condition of soil overburden are studied first. Both the FRP and stainless steel pipes are under non-operating and operating conditions.

The simulation results show that the highest soil stresses are found at the bottom strata due to the overburden load by the top strata. Under non-operating conditions, the maximum soil Mises stress with stainless steel pipe is approximately 114.6 kPa, which is about 28.9% lower than the corresponding case for FRP pipe (161.2 kPa).

The disparity between the two models increases greatly to approximately 90.8% (Steel: 114.6 kPa, FRP: 1.249 MPa) after pressurization of the pipe. This is due to interference fitting of the composite pipe joints, which causes the soil around the pipe joints to experience high localized stresses, which may be seen from Fig. 3.

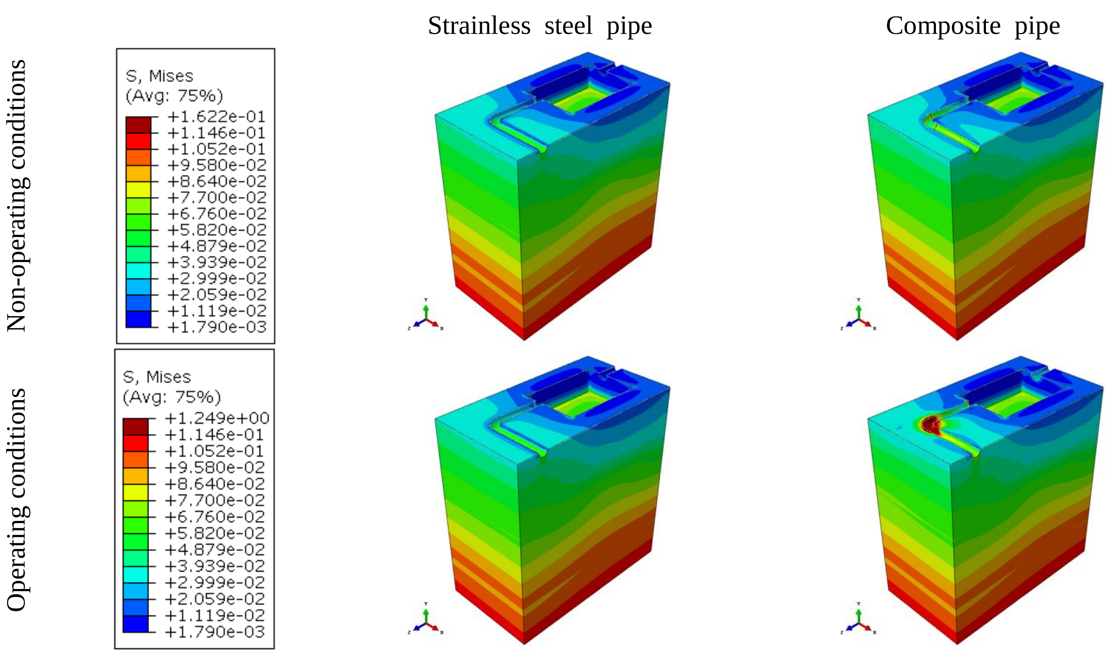

Fig. 3 Section views cut at the pipe middle section

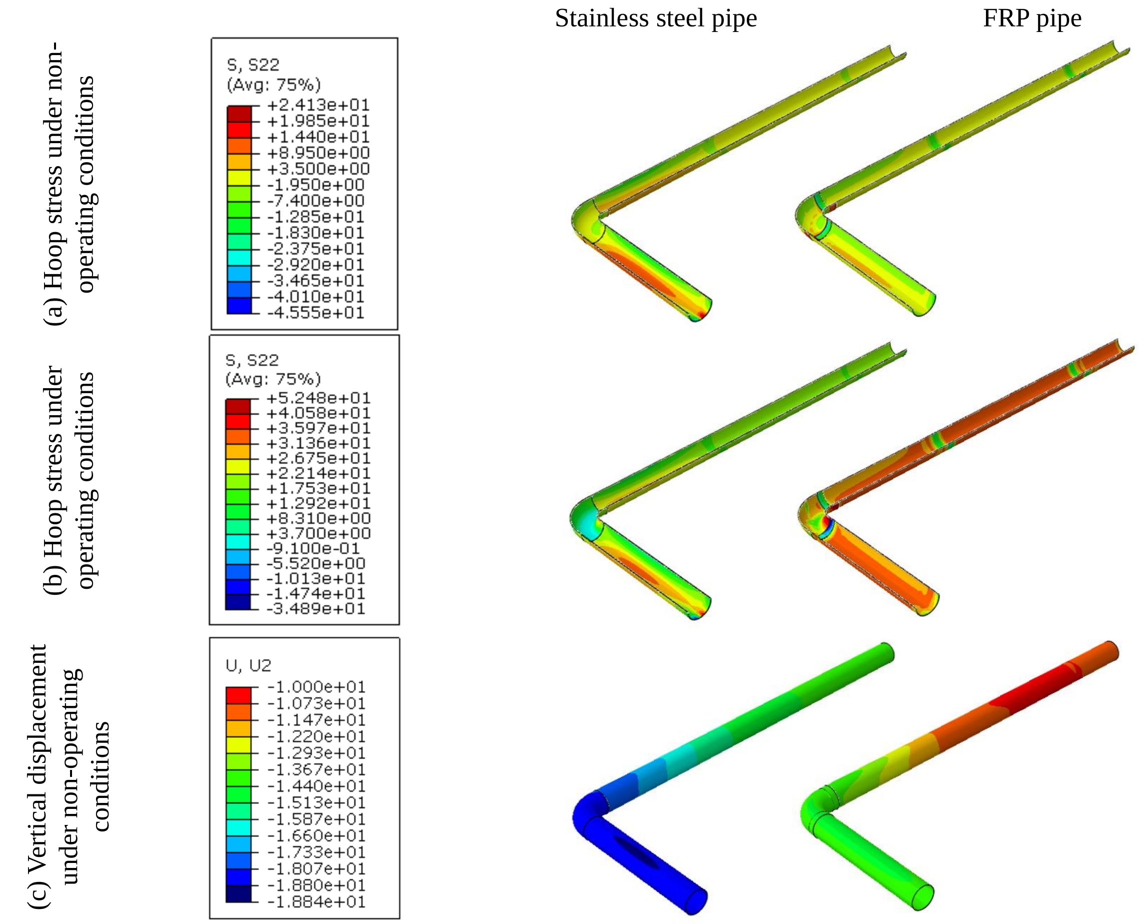

Fig. 4 Contour plots of (a) hoop stress under non-operating conditions, (b) hoop stress under operating conditions and (c) vertical displacement of both stainless steel and FRP pipes

Comparing between operating and non-operating conditions, the Mises stress contours of the near-field soil surrounding each pipe are generally identical throughout the models, except for higher stress near the soil-pipe interface.

Comparing between the steel and composite pipes, some difference in the stress contours can be observed, especially

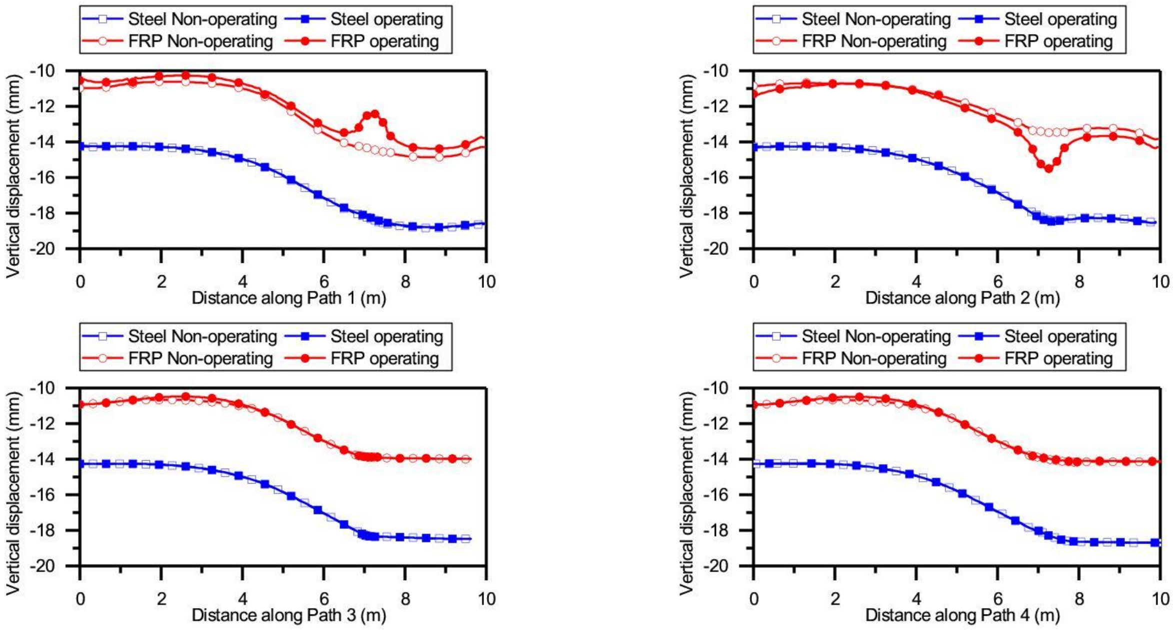

Fig. 5 Comparison of pipe vertical displacement (U2) along the stainless steel pipeline at various paths (Path 1: the crown, Path 2: invert, Path 3: inner springline and Path 4: outer springline) for both non-operating and operating conditions. 0m corresponds to end of longer pipe section away from the joint while 10m corresponds to the far end of the short pipe away from the joint

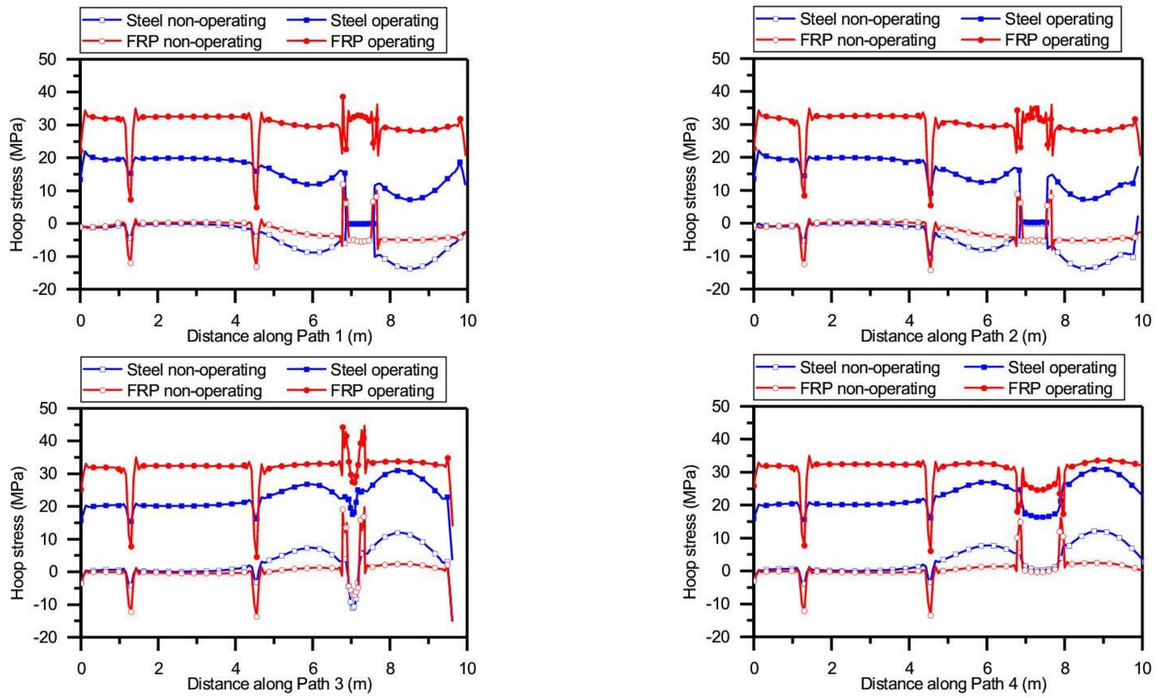

Fig. 6 Comparison of pipe hoop stresses (S22) along the steel pipeline at various paths (Path 1: crown, Path 2: invert, Path 3: inner springline, Path 4: outer springline) for both operating and non-operating conditions. 0m corresponds to end of longer pipe section away from the joint while 10m corresponds to the far end of the short pipe away from the joint

at the 90° elbow joint. This is due to additional stresses generated by the presence of the restraining bell-spigot joint.

Fig. 4(a) and (b) shows comparisons of hoop stresses in both pipes under both conditions. Higher magnitudes of hoop stresses are found at the pipe connections. Prior to pressurization, the steel pipeline have a maximum tensile hoop stress of 24.13 MPa, which is 17.7% higher than the FRP pipeline (19.85 MPa). This trend is reversed upon pressurization of the pipes, where the FRP pipeline (52.48 MPa) has a maximum hoop stress which is 22.7% higher than the steel pipeline (40.58 MPa). The higher stresses in the composite pipes is due to stress localization at the bell-spigot interference fitting, which is absent in the steel

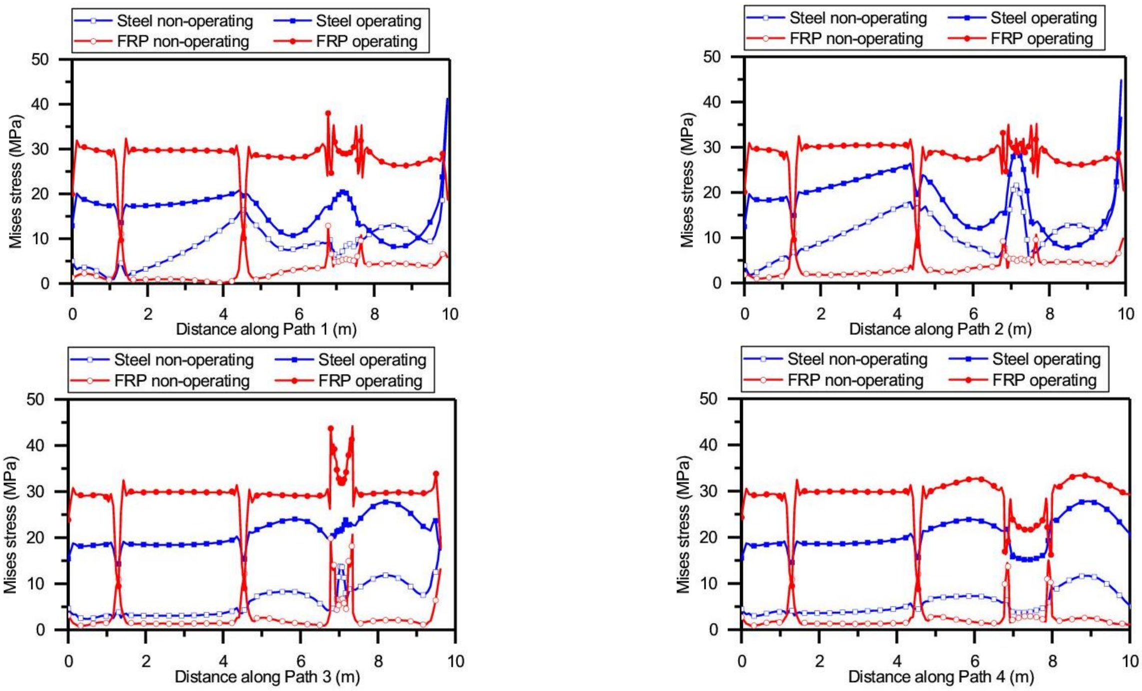

Fig. 7 Comparison of pipe Mises stresses along the steel pipeline at various paths (Path 1: crown, Path 2: invert, Path 3: inner springline, Path 4: outer springline) for both operating and non-operating conditions. 0m corresponds to end of longer pipe section away from the joint while 10m corresponds to the far end of the short pipe away from the joint

pipeline. However, , the maximum hoop compressive stress in the FRP pipe is higher than in steel pipe regardless of the operating conditions.

Fig. 4(c) shows the contour plots of vertical displacement of both the FRP pipe and the stainless steel pipe under non-operating condition. The *L*-shaped segment outside the valve pit sinks more than the pipe section that is inside the valve pit. This is due to the effect of topsoil overburden, where the weight of the soil above the pipe causes a larger downward force on the *L*-shaped pipe outside the pit than the pipe segment inside the pit. By comparing the relative vertical displacement of the two ends of the pipe, it is observed that the stainless steel pipe bends by 0.0115 d_0 while the FRP pipe bends by 0.0106 d_0.

Fig. 5 shows displacement path plots along the crown, invert and springlines of both pipelines under both conditions. The stainless steel pipe displaces almost identically for both operating and non-operating conditions. At the 90° elbow, the crown, invert and the springlines of the steel pipe displace around 18.5 mm and therefore there is no observable ovalization during both the non-operating and operating conditions.

This is in contrast to the response of the FRP pipe, where there is a significant difference in the vertical displacements at the joints on the crown and invert, under the two conditions. The vertical displacements at the crown and inverts of the FRP pipe joint show a divergence from the non-operating condition, apparent from the ‘humps’ between 6 to 8 m. This divergence indicate that the crown and invert positions become further away during operating conditions, thus ‘opening’ up the pipe-joint interface. This difference in response between pipes of the two materials indicates that the butt-welded steel pipe joint would not “open” up like the interference fitted bell-and-spigot joint in the FRP composite pipe. The comparison of the hoop stresses plots along the crown, invert and springlines of the pipeline is shown in Fig. 6.

The variation in stainless steel pipe hoop stresses under non-operating and operating conditions are generally found to be about 20 MPa (comparing to 30 MPa for FRP pipe), except for the elbow’s crown and invert. Similarly, axial stresses S33 at operating condition are found to be about 7-8 MPa higher than that of the non-operating condition.

Generally, the stress values are slightly lower at both pipe-pit penetrations during both non-operating and operating conditions. This may be tempting to infer that the soil load would be more damaging than the compressible external forces induced by the MCT rubber.

Fig. 7 depicts the comparison of the plots of Mises stress distribution along the crown, invert and springlines of the steel pipeline. The stress variation, between non-operating and operating conditions, varies by a substantial amount along the steel pipes at its crown and invert positions, with the largest stress variation of 15-20 MPa at the longer end, whereas there is insignificant stress variation at the shorter end. This is not the case with the springlines, where the pipe stresses at the two springlines for operating condition are generally about 15-20 MPa higher than that of non-operating condition, except for the 90° elbow, the pipe end of the short pipe segment and at the pipe supports. As for the FRP pipe, the stress during operation is generally about 25-30 MPa higher than non-operating conditions, except at the elbow, short end of pipe and at the pipe supports.

Table 4 shows a summary of the comparison of the pipe responses for both the FRP and stainless steel pipes. The

Table 4 Pipe response for FRP and stainless steel pipes under effect of topsoil overburden. Stress values are also presented as percentages of the material strengths in the parenthesis

	FRP		Stainless steel	
	Non-operating	Operating	Non-operating	Operating
Max. tensile hoop stress (MPa)	19.84 (9.02%)	52.48 (23.85%)	24.13 (4.98%)	40.58 (8.37%)
Max. compressive hoop stress (MPa)	45.54 (20.70%)	34.89 (15.86%)	31.22 (6.44%)	14.74 (3.04%)
Max. tensile axial stress (MPa)	11.76 (19.93%)	18.39 (31.17%)	20.46 (4.22%)	31.37 (6.47%)
Max. compressive axial stress (MPa)	13.61 (23.07%)	11.8 (20.00%)	24.09 (4.97%)	15.19 (3.13%)
Max. relative vertical displacement (mm)	4.25	6.22	4.59	4.59

stainless steel pipe section modelled in this investigation is also unlikely to fail under both non-operating and operating conditions as the maximum stress fall below the threshold limits. For FRP pipes under overburden load, the maximum tensile hoop stress experienced is found to be 23.85% of the threshold of 220 MPa, while the maximum tensile axial stress is 31.17% of failure threshold in axial direction (59 MPa). For stainless steel pipes under overburden load during operation, the maximum tensile hoop stress experienced is 23.87% of its yield strength (170 MPa) and 8.37% of its ultimate tensile strength (UTS) (485 MPa). The maximum tensile axial stress is 18.45% of yield strength (170 MPa) and 6.47% of the UTS (485 MPa).

The Mises stress experienced by the operating stainless steel pipe is found to be around 10.34% of the ultimate tensile strength of stainless stain. It is surmised that using stainless steel pipes afford a greater safety factor than FRP pipe. However, the study does not take into account temperature effects and corrosion. Metallic structures are known to be more prone to damage by temperature changes such as freezing and condensation, as well as corrosion. Fiberglass composites, which are lighter, highly corrosion and abrasion resistant, may offer a better alternative in the current application, despite its weaker strengths (as compared to stainless steel).

3.2 Effect of loose bed-soil support on buried composite pipe

Fig. 8 shows the Mises stress contours of the soil at the pipe middle section for both cases of fully supported and partially supported pipes. It can be seen that the soil stresses in the case of loose bed-soil support show a larger variation between the minimum and maximum values. The peak soil stress, near the 90° elbow, for the current case is 10.73% higher compared to the fully-supported pipe case which experiences only fitting stresses and geostatic load.

Fig. 9 shows the maximum vertical ground settlement for the non-operating case. The loss of bed soil support results in larger vertical soil settlement at the ground directly above the affected region. The soil settles by a further 2.3 mm, which will likely cause the pipe at the pit-pipe penetration to experience more severe bending.

Fig. 10 shows the hoop and axial stresses of the buried composite FRP pipe for the operating case.

Higher hoop stresses are found at the inner bend surface of the 90° elbow joint, with the maximum tensile stress of around 79.38 MPa in the case of loose bed-soil support, and

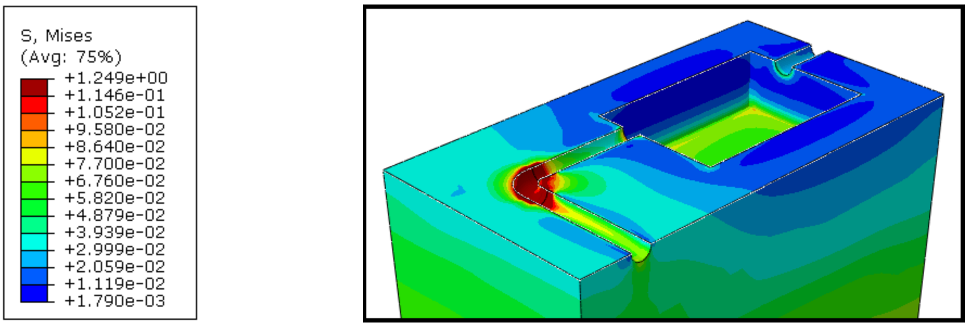

(a) Supported pipe

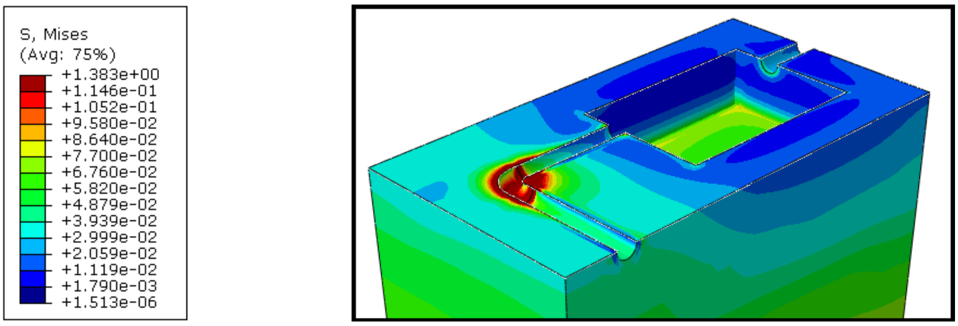

(b) Pipe with loose bed-soil support

Fig. 8 Mises stress contours of the soil at pipe middle section for the FRP pipe with (a) fully supported bed-soil, and (b) loose bed-soil support

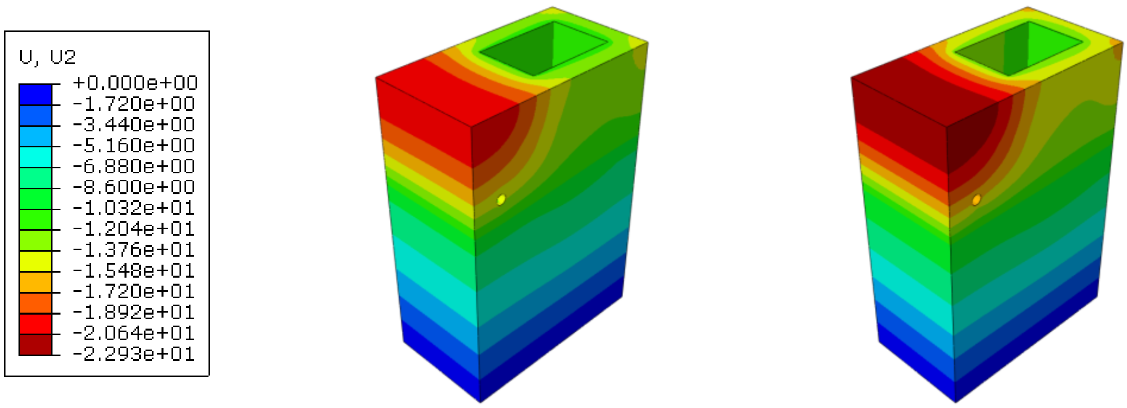

(a) (b)

Fig. 9 Vertical soil settlement for the FRP pipe with (a) fully supported bed-soil, and (b) loss of bed-soil support

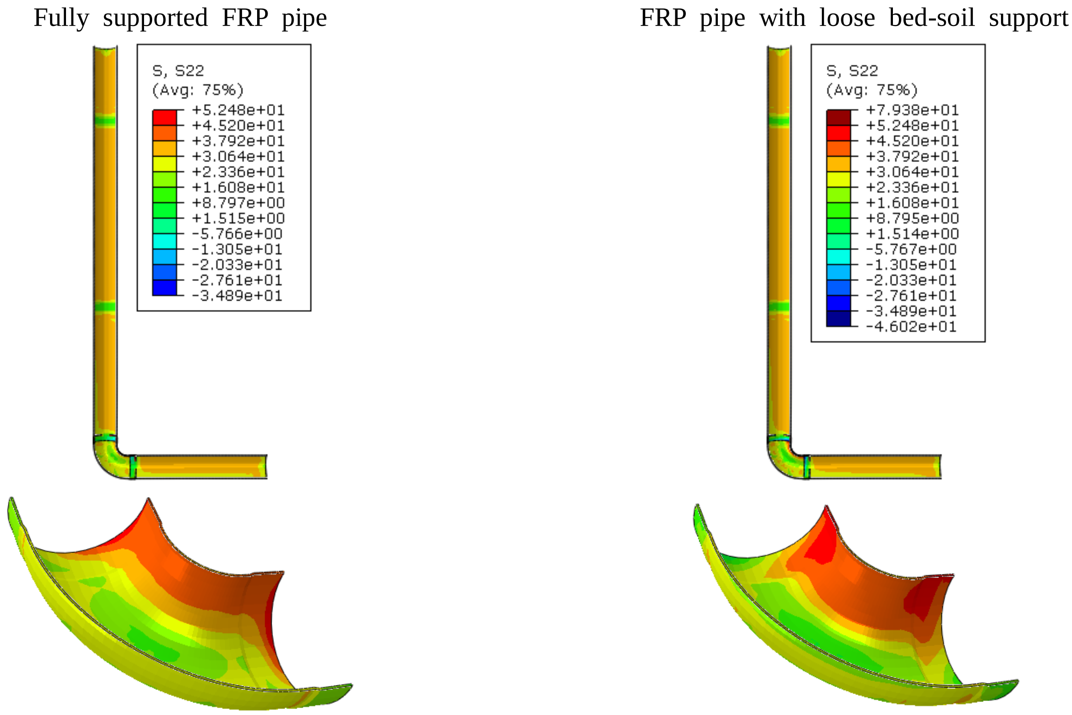

Fig. 10 Hoop stress (S22) contours of the pipes under effect of loss in bed-soil support and internal pressurization; enlarged pictures show the maximum stress in the interior surface of the bell at the inner bend

52.48MPa for the case of full bed-soil support. The corresponding maximum compressive hoop stresses are -46.02 MPa and -34.89 MPa respectively. The former value is a 31.8% increase compared to the fully supported scenario with pressurized pipeline. For all scenarios and cases, relatively lower hoop stresses are obtained at the pipe-pit penetration as compared to the pipe body.

In general, the exterior surface of the inner bell portion of the pipe connection experiences high tensile hoop stress while the inner spigot portion experiences the highest compressive hoop stress. For the operating case, the inner pipe bend is observed to experience higher hoop stresses than the outer pipe bend.

Fig. 11 shows the displacement magnitude and vertical displacement contours of the affected pipeline during operation. The two plots are almost identical with a slight difference at the elbow. The *L*-shaped segment which is outside the valve pit and spanning over the loss bed support region is observed to sink more and experience larger pipe displacements compared to the full bed support scenario. High axial displacements at the joints are shown by the higher displacement magnitudes at these locations. With the loss of bed support over the *L*-shaped pipe segment, its relative vertical displacement with respect to the other supported end is approximately 6.8 mm, which is about 9% higher when compared to the fully supported case of 6.2 mm. For the non-operating case, the maximum relative pipe displacement is 5.45 mm which is 28.24% higher than the corresponding fully supported case of 4.25 mm.

The hoop and axial stresses along the pipeline are presented in Figs. 12 to 14 respectively. The pipe-body hoop and axial stresses at the operating condition are found,

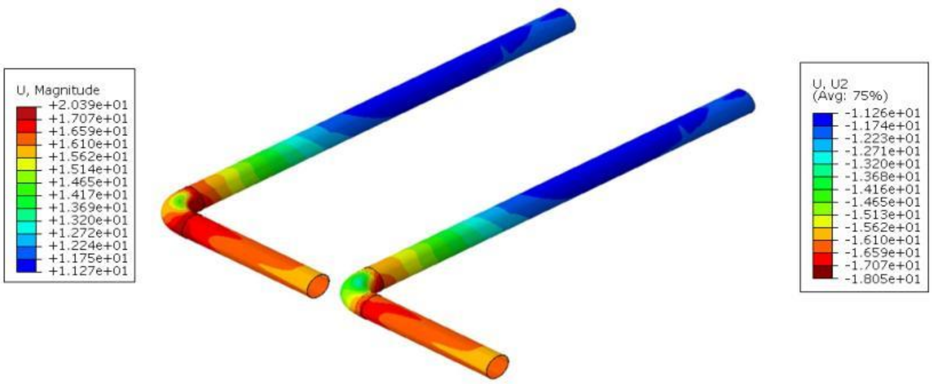

Fig. 11 Displacement magnitude and vertical displacement (U2) of the affected pipe segment due to operating pressure and loss in bed-soil support

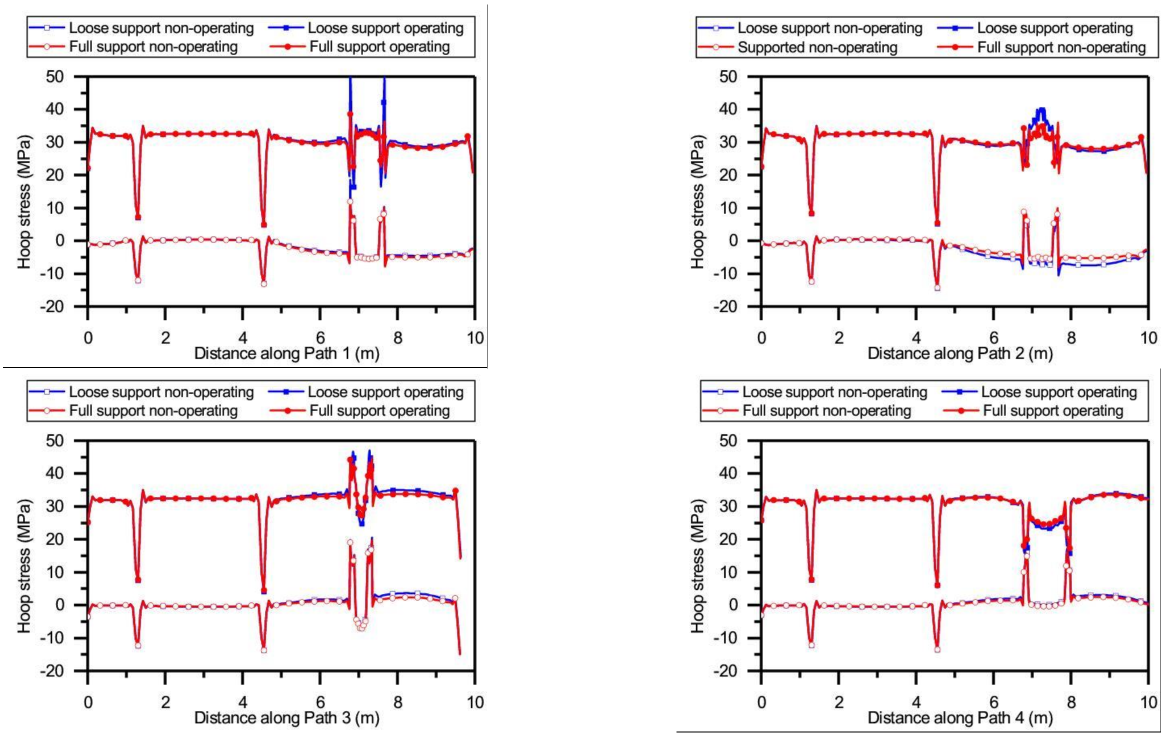

Fig. 12 Comparison of hoop stress along pipeline at various paths (Path 1: crown, Path 2: invert, Path 3: inner springline, Path 4: outer springline). 0m corresponds to end of longer pipe section away from the joint while 10m corresponds to the far end of the short pipe away from the joint

respectively, to be about 30 MPa and 6 MPa higher than those from the non-operating condition. Lower hoop stress differences of about 20 MPa are found at the pipe-pit penetration between operating and non-operating conditions as the MCT rubber restricted the pipe from naturally expanding. The interference fitted joints are observed to experience less hoop stress differentials across the non-operating and operating states, due to their greater overall thickness. For axial stress distribution, the stresses hover around 6 MPa before ramping up at the 90^o bend. Unlike the fully supported case, the pipe section experiences a larger change in axial stresses during switching between states. The stress differentials are around 15 MPa for the fully supported case and 20 MPa for the case of loss in bed-soil support. The effects of loose bed-soil can be seen to be insignificant with respect to causing failure of the pipes, as the increased stresses experienced by the pipe are still significantly lower than the strength of the pipe. Considering loss of bed-soil as a major effect of geotechnical catastrophes such as earthquakes and landslide, the FRP pipeline possesses good axial deformation capabilities. However, it should be noted that earthquakes are dynamic in nature and may therefore cause failures in the pipeline through other mechanisms which are not modelled in the current model.

However, it is noted that for some of the paths, stresses may fluctuate between tensile and compressive during mode switching. The difference between the tensile and compressive stresses increases for the case of loss of bed-soil support. As a consequence, in the case of loss of bed-soil support, there is a higher possibility for the affected pipe section to experience fatigue failure if frequent mode

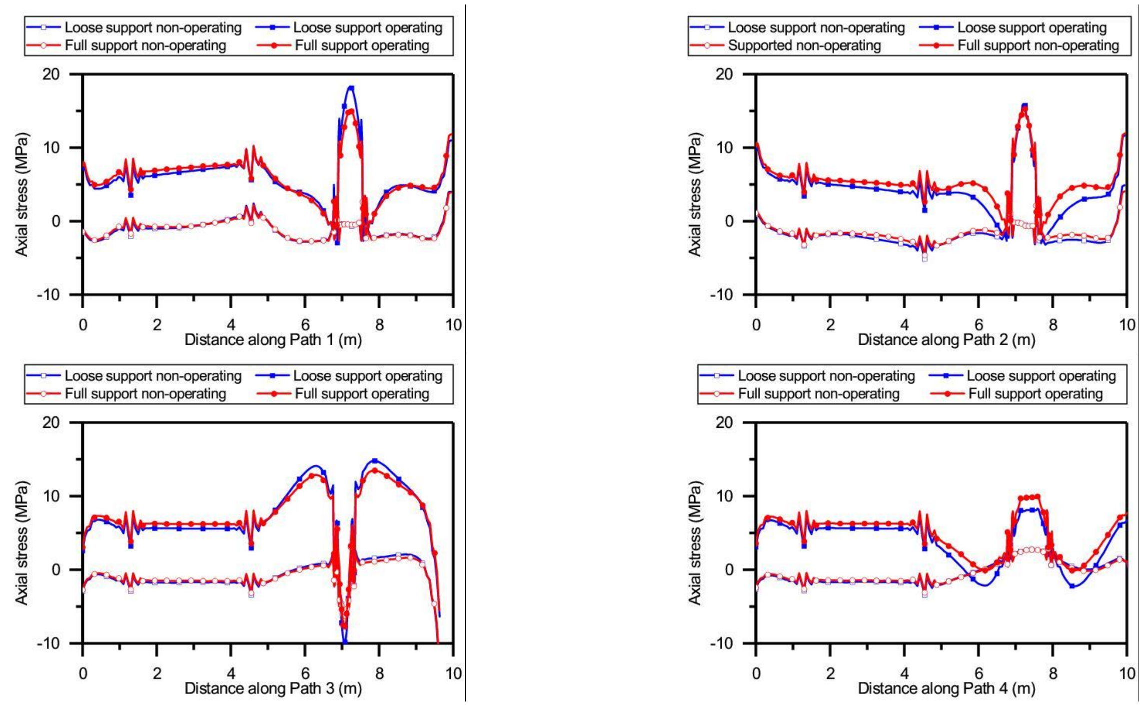

Fig. 13 Comparison of axial stress along pipeline at various paths (Path 1: crown, Path 2: invert, Path 3: inner springline, Path 4: outer springline). 0m corresponds to end of longer pipe section away from the joint while 10m corresponds to the far end of the short pipe away from the joint

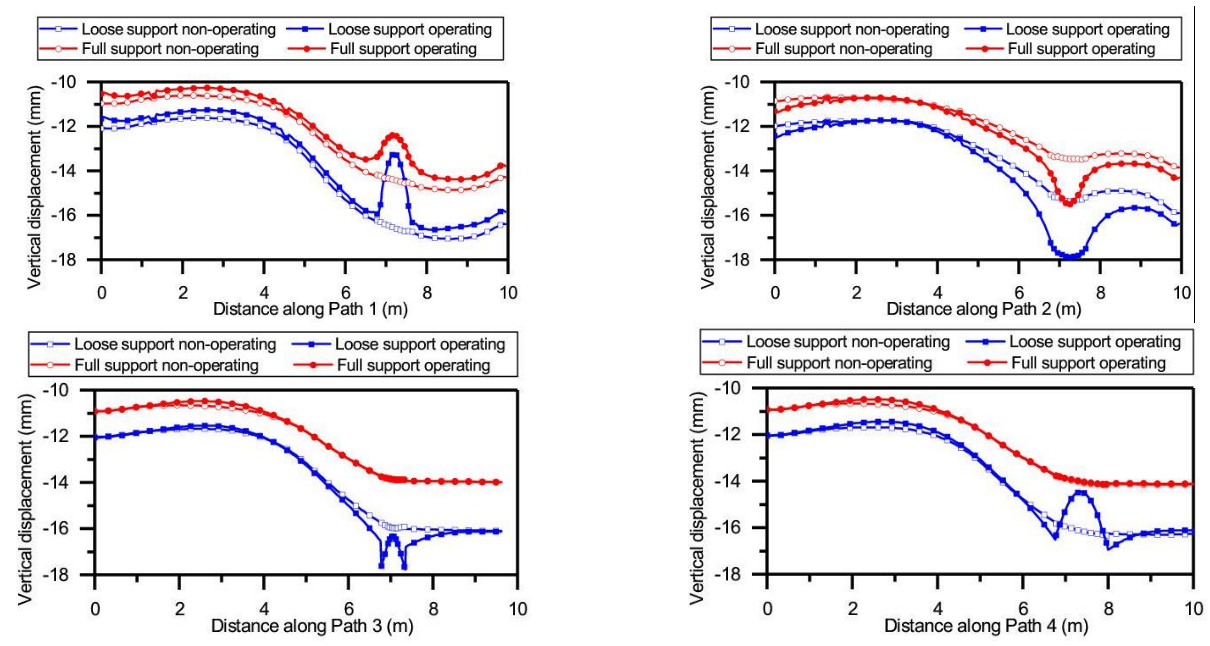

Fig. 14 Comparison of pipe vertical displacement along the pipeline at various paths (Path 1: crown, Path 2: invert, Path 3: inner springline, Path 4: outer springline). 0m corresponds to end of longer pipe section away from the joint while 10m corresponds to the far end of the short pipe away from the joint

switching has to be performed through the pipeline's lifetime.

Fig. 14 shows the displacement distribution along the pipeline whereby the pipe section within the pit perimeter is found to have been displaced by about 12 mm while sections further away displaces more (about 16-17 mm). This is expected as the soil weighs down on the partially supported pipe, while the pit is primarily hollow and tends to sink less. It is also noted that during operations, the crown yielded a lower vertical displacement than the invert at the unsupported 90^o elbow, which leads to an ovalization of more than 5 mm during pipe pressurization. There is a difference in pipe vertical displacement between the two springlines, implying that torsion of the pipe is evident at the 90 degrees bend.

In addition, to determine if the pipe connections are still

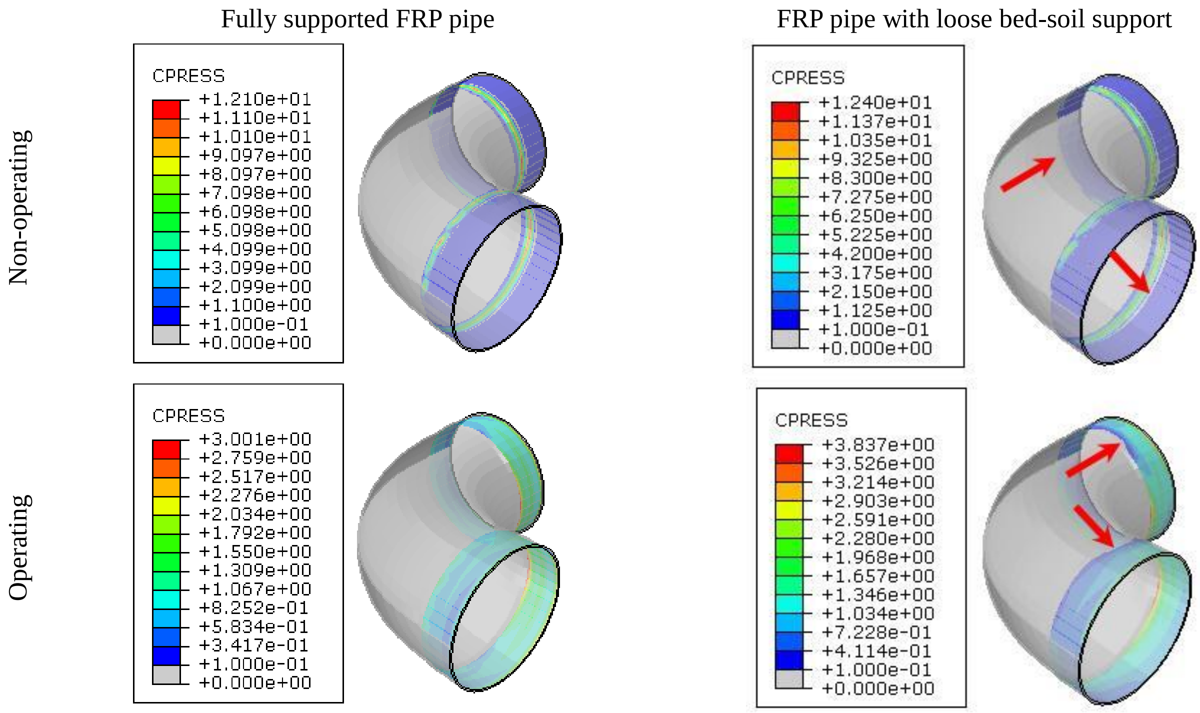

Fig. 15 Contact pressure contours at the pipe connections of the 90^{o} bend under operating and non-operating conditions. Note: zero contact pressure is found at the inner elbow bell's edge indicated by red arrows

intact, the contact pressures of the pipe junctions are checked. Positive contact pressures imply intact interfaces while zero contact pressure implies open contact. Fig. 15 shows contact pressure contours in the elbow joints for both cases with full and partial bed-soil support and with and without pipe pressurization. It is observed that in the case of loose bed-soil support, there is zero contact pressure at parts of the joints, as highlighted by the arrows. This implies that these contact regions are not intact despite the pressurization step which aids in closing up initially open regions at the bend. This observation is different from the fully supported case where the internal pressurization helps to close up the gap completely. This is intuitive as the elbow connection in the partially supported pipeline would have opened up more due to greater ovalization at the bend due to the overburden load.

When compared to the fully supported scenario, the current cases with a loss in bed-soil support yielded more regions with lower or zero joint contact pressure which indicated that the effect of bed-soil loss could be the opening up of connections at critical bends. Comparing the cases with and without pipe pressurization, it was found that pipe pressurization helped improve the contacts at the joint interfaces at the elbow for the fully soil-supported case, but did not help as much for the case with a loss in bed-soil support. This is intuitive as the loss of bed-soil support would result in greater bending and ovalization of the pipe, thus resulting in pipe pressurization not being able to help in closing up the contact at the joints, as in the case of the fully supported pipe. This also serves to highlight that pipe pressurization would not improve the pipeline conduit integrity if larger deformations, such as due to loss in bed-soil, are encountered.

4. Conclusions

The paper has investigated the response of both composite and steel pipelines due to the effects of gravity and geostatic stresses through numerical means. In addition to comparing the difference between steel and composite pipes, the paper has also investigated the effects of loss of bed-soil support, which may be present during landslides or severe rainfall.

In comparing the differences between steel and composite pipes. The simulation results provided insights to the response of buried composite pipes and in particular the pipe-soil interaction that occurs for mutual transfer of loads between soil and pipe. The differences in response between cases with steel and composite pipes under operating and non-operating conditions were first considered. Results revealed that internal pressurization reduces pipe ovalization due to overburden loads but results in increased pipe axial stresses at pipe bends. With the bell and spigot connections, the location of lowest contact pressure is the inner springline of pipe bend interfaces, and has been identified as the possible location for leakage. It was shown that considering mechanical effects alone, the steel pipe offers better performance. However, in the design phase of a pipeline, steel pipes may not offer as much advantage due to other factors, such weight of the pipes, logistics and cost of transportation, additional procedures for pipe laying, corrosion and thermal expansion, for which composite pipes may offer a better option.

In the scenario of a loss in bed-soil support for the buried pipe. The simulation results revealed significant settlement of the ground. Higher pipe axial tensile stresses at the crown and invert are induced at regions near to the edge of the lost soil block. This increase in stresses however, are insignificant in causing failure of the pipe structure. Notwithstanding, it has to be noted that the pipe connections lacking bed-soil support will experience larger vertical displacements which will tend to open up the joints, causing leaking due to connection failures rather than material failure.

Acknowledgements

The support of Defence Science and Technology Agency (DSTA), Singapore, under project grant number R-379-000-031-422 for this work is gratefully acknowledged.

References

Almahakeri, M., Moore, I.D. and Fam, A. (2012), "The flexural behavior of buried steel and composite pipes pulled relative to dense sand: experimental and numerical investigation", *Proceedings of the 9th International Conference on Pipelines IPC2012*, Calgary, Alta.

Alzabeebee, S. (2016). "Investigating the response of rigid pipes with poor haunch support subjected to trafficlive load using numerical modeling", *11th Pipeline Technology Conference*, Berlin, Germany.

Ameron (2008), *Bondstrand 2000, 4000 and 7000 Glass Fiber Reinforced Epoxy (GRE) Pipe Systems for General Service*, The Netherlands.

Armstrong, K.B., Bevan, L.G. and Cole, W.F. (2005), *Care and Repair of Advanced Composites*, SAE International

Bai, Y., Yuan, S., Cheng, P., Han, P., Ruan, W. and Tang, G. (2016), "Confined collapse of unbonded multi-layer pipe subjected to external pressure", *Compos. Struct*., **158** 1-10.

Beckwith, S. and Greenwood, M. (2006), *Don't Overlook Composite FRP Pipe*,

Bryan, J.J. (1956), "The investigations, design and construction of Paya Lebar Airport, Singapore", *Proc. Inst. Civil Eng*., **5**(5), 379-408.

Chapman, D., Alzabeebee, S., Jefferson, I. and Faramarzi, A. (2016). "Investigating the maximum soil pressure on a concrete pipe with poor haunch support subjected to traffic live load using numerical modelling", *11th Pipeline Technology Conference*, Berlin, Germany.

Chen, L.Q., Wu, S.J., Lu, H.F., Huang, K. and Shi, J.Y. (2014), "Comparative analysis of FRP and seamless steel pipe on crude oil transportation performance", *J. Chem. Pharmaceut. Res*., **6**(7), 2364-2369.

Elachachi, S.M., Breysse, D. and Denis, A. (2012), "The effects of soil spatial variability on the reliability of rigid buried pipes", *Comput. Geotech*., **43** 61-71.

Gantes, C. and Melissianos, V. (2016), *Evaluation of Seismic Protection Methods for Buried Fuel Pipelines Subjected to Fault Rupture*,

Gantes, C.J. and Melissianos, V.E. (2016), "Evaluation of seismic protection methods for buried fuel pipelines subjected to Fault rupture", *Front. Built Environ*., **2**, 1-12.

Gong, S.F. and Hu, Q. (2014), "Buckling and collapse analyses of composite structures for deepwater sandwich pipes under external pressure", *J. Zhejiang Univ*., **48**(9), 1624-1631.

Jones, R.M. (1998), *Mechanics of Composite Materials*, CRC press

Khemis, A., Chaoche, A.H., Athmani, A. and Tee, K.F. (2016), "Uncertainty effects of soil and structural properties on the buckling of flexible pipes shallowly buried in Winkler foundation", *Struct. Eng. Mech*., **59**(4), 739-759.

Lee, Y.G., Kim, S.H., Park, J.S., Kang, J.W. and Yoon, S.J. (2015), "Full-scale field test for buried glass-fiber reinforced plastic pipe with large diameter", *Compos. Struct*., **120** 167-173.

Liu, H. (2009), "Dynamic analysis of subway structures under blast loading", *Geotech. Geol. Eng*., **27**(6), 699.

Mahdi, M. and Katebi, H. (2015), "Numerical modeling of uplift resistance of buried pipelines in sand, reinforced with geogrid and innovative grid-anchor system", *Geomech. Eng*., **9**(6), 757-774.

Olarewaju, A.J., Kameswara Rao, N.S.V. and Mannan, M.A. (2010), "Response of underground pipes due to blast loads by simulation - An overview", *Elect. J. Geotech. Eng*., **10**(H), 831-852.

Olarewaju, A.J., Rao, N.S.V.K. and Mannan, M.A. (2010), "Blast effects on underground pipes", *Elect. J. Geotech. Eng*., **15** 645-658.

Olarewaju, A.J., Rao, N.S.V.K. and Mannan, M.A. (2010). "Design hints for buried pipes to resist effects of blast", *Indian Geotechnical Conference (GEOtrendz)*, Bombay, Indian.

Olarewaju, A.J., Rao, N.S.V.K. and Mannan, M.A. (2010), "Simulation and verification of blast load duration for studying the response of underground horizontal and vertical pipes using finite element method", *Elect. J. Geotech. Eng*., **16** 12.

Rafiee, R. and Mazhari, B. (2016), "Simulation of the long-term hydrostatic tests on glass fiber reinforced plastic pipes", *Compos. Struct*., **136** 56-63.

Rajeev, P. and Kodikara, J. (2011), "Numerical analysis of an experimental pipe buried in swelling soil", *Comput. Geotech*., **38**(7), 897-904.

Schmmit, K. (1998), *Fiberglass Reinforced Plastic (FRP) Piping Systems Designing Process/ Facilities Piping Systems with FRP: A Comparison to Traditional Metallic Materials*, Fiberbond

Soheyli, M.R., Akhaveissy, A.H. and Mirhosseini, S.M. (2016), "Large-scale experimental and numerical study of blast acceleration created by close-in buried explosion on underground tunnel lining", *Shock Vib*., **2016**, Article ID 8918050.

Song, B. and Chen, W. (2003), "One-dimensional dynamic compressive behavior of EPDM rubber", *J. Eng. Mater. Technol*., **125**(3), 294-301.

Taheri, F. (2013), *18-Advanced Fiber-Reinforced Polymer (FRP) Composites for the Manufacture and Rehabilitation of Pipes and Tanks in the Oil and Gas Industry A2 - Bai, Jiping*, Woodhead Publishing.

Tan, L.B., Tse, K.M., Tan, V.B.C. and Lee, H.P. (2015), *Finite Element Modeling of Buried Glass Reinforced Composite Pipe*, Lisboa, Portugal.

Trifonov, O.V. and Cherniy, V.P. (2012), "Elastoplastic stress-strain analysis of buried steel pipelines subjected to fault displacements with account for service loads", *Soil Dyn. Earthq. Eng*., **33**(1), 54-62.

V-PILE (2011), *Soil Investigation Report (Kaki Bukit Road 4/ Bartley Road East)*, Singapore.

Vazouras, P., Karamanos, S.A. and Dakoulas, P. (2010), "Finite element analysis of buried steel pipelines under strike-slip fault displacements", *Soil Dyn. Earthq. Eng*., **30**(11), 1361-1376.

Vazouras, P., Karamanos, S.A. and Dakoulas, P. (2012), "Mechanical behavior of buried steel pipes crossing active strike-slip faults", *Soil Dyn. Earthq. Eng*., **41** 164-180.

Watkins, R.K. and Anderson, L.R. (1999), *Structural Mechanics of Buried Pipes*, Taylor & Francis

CC